DOI: 10.31534/engmod.2024.1.ri.03v
Original scientific paper
Received: 12.06.2023.

High Impedance Arc Fault Modelling in Offshore Oil Platform Power Grid

Yonghu Wu(1,*), **Cun Huang**(1), **Fen Dong**(1), **Guoxiang Li**(1), **Gaowei Wang**(2), **Sai Zhang**(2), **Tong Zhao**(2)

(1,*) *China National Offshore Oil Corporation Limited, Beijing 100020, CHINA*
Correspondence author: e-mail: wuyh10@cnooc.com.cn

(1) *China National Offshore Oil Corporation Limited, Beijing 100020, CHINA*
e-mails: huangcun@cnooc.com.cn; dongfen@cnooc.com.cn; ligx21@cnooc.com.cn

(2) *North China University of Technology School of Electrical and Control Engineering, Beijing 100144, CHINA*
e-mails: wgw_686@163.com; 2072774451@qq.com; 862255299@qq.com

SUMMARY

In offshore oil platform power grid, high impedance arc fault occurs frequently. The fault characteristics of high- impedance arc information are weak and difficult to detect, which may not cause the protection method to activate. Therefore, it is important to detect and clear the high impedance fault. In the high impedance case, usually, the arc fault occurs. In the research, the arc model was established using the typical Cassie model and the high impedance arc fault characteristics in offshore oil platform power grids were analysed. An improved arc fault detection method using the phase angle difference between zero sequence voltage and zero sequence current was proposed to extract fault characteristics. This method requires limited detection information and high accuracy to solve the problem of small current and voltage changes in high-resistance arc faults. The offshore oil platform power grid and the arc were modelled using electromagnetic transients software PSCAD/EMTDC. The simulation results show that the arc model and fault detection method work well.

KEY WORDS: *offshore power grid; high impedance fault; Cassie model; PSCAD/EMTDC.*

1. INTRODUCTION

The power grid of offshore oil platforms contains a variety of power electronic equipment and diesel generators that mostly operate in small areas, so the working environment is relatively specific. The environmental conditions are relatively poor [1]. When using the platform grid for power supply, it is easy to cause faults due to broken line insulation, environment, and other factors.

Offshore oil platform power grid faults can be classified as line-to-line faults and line-to-ground faults. According to the location, they are divided into distribution line fault, power generation

element faults, energy storage element faults, converter faults, etc., and according to the fault impedance, into metal faults, and various faults with a certain resistance value. It is generally considered that fault transition resistance above 300 ohm is a high-impedance fault.

After the metal fault or small impedance fault occurs in the power grid of the platform, the fault characteristics are obvious, and the electrical characteristics change drastically enabling the fault to be detected and eliminated quickly. However, if the resistance is too large when a fault occurs in the offshore oil platform power grid, there is no significant difference in electrical quantities and the fault characteristics are not obvious, so it is difficult for the control and protection equipment of the power grid in the offshore oil platform to detect the fault state [2-3].

In the power grid in offshore oil and gas platforms, many cases can occur where high impedance faults are likely to occur, such as the insulation damage of the line cable caused by the humid environment, the aging and loosening connector, and electric shock in the line through organisms. Since the high impedance fault is difficult to detect, it will exist for a long time. If there is an arc, it will hardly self-extinguish. In addition, the resistance of the cable is small. The fault can spread from one position through the whole system and damage the equipment and human safety. Therefore, it is necessary to detect the high-impedance fault in the offshore oil platforms [4-6].

High impedance fault usually occurs as arc type. The resistance is nonlinear with a large value. Therefore, the current is small and difficult to be detected [7-8]. The simulation model of the grounding arc is represented by Cassie mathematical model and Mayr mathematical model in the field of high-voltage electrical insulation. Cassie model is usually used to describe the arc resistance at a large zone, while Mayr model describes the arc resistance at a small zone. The arc resistance is time-varying, and the range of resistance changes across the low-resistance and high-resistance regions. Because of the zero-crossing phenomenon of AC voltage and current, the arc will be accompanied by an intermittent "extinction reignition" process [9-11].

The existing arc fault detection methods consist of the arc characteristic identification method, voltage vector analysis method, etc. However, it is difficult to set the threshold value of this method. In the case of large grounding resistance faults, it is difficult to distinguish them from the normal working state, which leads to default initialization of the starting criteria. Because the starting criteria and the distinguishing criteria are not established separately, the overall detection accuracy is low in case of high impedance fault, but establishing different criteria has no physical significance and requires a large amount of calculation.

Ref. [12] proposes a high resistance dual wire grounding fault detection method in electrical transmission based on a grounding resistor placed at the midpoint of the DC side, which can detect the starting area of the dual wire grounding fault and identify the DC fault pole or AC fault phase. However, the exact position of each ground fault is still unknown.

Ref. [13] adopts Mayr model to make a detailed analysis. By processing the voltage drop during the fault, the zero sequence current is extracted to rate the interrupting ability of the current after the fault. The final results of processing can be combined with other models for estimation and rating. However, the applicability of the arc model of this method needs further research and may not be suitable for special environments such as offshore oil platforms and islands.

Ref. [14] proposes a fault detection index by using the correlation between the DC capacitor power and the line power of the system. The proposed method has significant characteristics such as fast fault detection speed, accurate differentiation of faulty and healthy transmission lines, coverage of high resistance arc faults, noise resistance, robustness to the system and signal

condition, without any additional sensors and communication infrastructure. However, the effectiveness of this method needs further verification.

In conclusion, the existing high-resistance characteristic analysis can not be appropriately applied to offshore oil platforms. Therefore, the paper analyses the high impedance arc fault characteristics in the offshore oil and gas platform power grids and completes the simulation model in the PSCAD/EMTDC. The fault characteristics show that the theory analysis is correct. The main contribution is shown below:

- A high-resistance fault simulation model based on Mayr model is suitable for special scenarios such as offshore oil platforms and islands.
- A fault interval positioning method based on voltage and current phasor characteristics is proposed.
- The fault interval positioning method uses the discrete Fourier transform (DFT), with a low sampling frequency and easy engineering implementation.
- A precise offshore oil platform was built using PSCAD/EMTDC electromagnetic transient simulation software.

The paper is as follows: section 1 analyzes high impedance arc fault modelling; section 2 describes the offshore oil platform power grid modelling and fault characteristics; simulation results for a power grid and fault detection are shown in section 3, and the conclusions are shown in section 4.

2. HIGH IMPEDANCE ARC FAULT MODELLING

The value of arc resistance is restricted by the voltage between arcs, direct current, air gap, and other environmental factors [15]. The expression of arc resistance combines the arc voltage and arc current. Also, the arc energy needs to be considered. The arc energy during the fault is shown in the Eq. (1):

$$\frac{dQ}{dt} = u \cdot i - P \tag{1}$$

Where Q represents the arc energy, P is the energy loss, u is the arc voltage and i is the current. Equation (1) can be further transformed into the relationship between the change rate of arc unit conductivity g and the change of arc power, as shown in Eq. (2) and Eq. (3):

$$\frac{dQ}{dt} \cdot \frac{dg}{dt} = \frac{1}{P^{-1}} \left(\frac{g \cdot u^2}{P} - 1 \right) \tag{2}$$

$$\frac{1}{g} \cdot \frac{dg}{dt} = \frac{1}{g \cdot P^{-1} \cdot \left(\frac{dQ}{dg} \right)} \left(\frac{g \cdot u^2}{P} - 1 \right) \tag{3}$$

Suppose that $\tau = g \cdot P^{-1} \cdot \frac{dQ}{dg}$, Eq. (3) can yield to Eq. (4):

$$\frac{d \ln g}{dt} = \frac{1}{\tau} \left(\frac{g \cdot u^2}{P} - 1 \right) \tag{4}$$

In Eq. (4), E represents the voltage gradient, P_0 is emitted power in the per unit volume, and $\sigma$is conductivity of the arc. The mathematical expression is shown below:

$$E^2 = \frac{P_0}{\sigma} \tag{5}$$

The following formula can be obtained through the analysis of Eq. (4) and Eq. (5):

$$\frac{d\ln g}{dt} = \frac{1}{\tau_c}\left(\frac{u^2}{E^2} - 1\right) \tag{6}$$

where τ_c represent Cassie model time constant. The arc resistance is shown in Eq. (7):

$$R_{arc} = e^{\frac{1}{\tau_c}\int(1-\frac{u^2}{E^2})dt} \tag{7}$$

In the high impedance fault, the arc is generated by air gap breakdown. The line and the grounding medium generate the arc with the resistance between the line and the grounding point.

The Cassie model shows that when the inter voltage reaches the arc voltage gradient, the arc current enters a stable combustion state. The arc resistance will consume a certain amount of energy, resulting in a small arc current, while the total resistance is large during the fault [16].

3. OFFSHORE OIL AND GAS PLATFORM POWER GRID MODELLING

The offshore oil and gas platform power grid contains diesel generators, cables, loads, and transformers [17]. Distributed generation, such as wind generators and photovoltaics, is interconnected to the power grid. The voltage level in the offshore power grid is *10 kV*, and the system is an ungrounded system. The fault current of the single line to ground fault (SLG) is quite small. The simplified diagram of the offshore oil and gas platform power grid is shown in Figure 1 below.

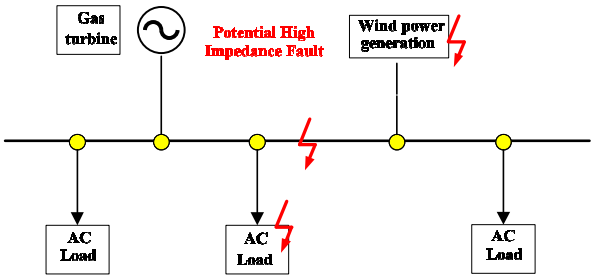

Fig. 1 *Schematic diagram of offshore oil and gas platform power grid*

The mathematical model of the gas turbine is as follows.

The outlet temperature value of the pressurizer for each segment is:

$$T_{out} = T_{in}\left[1 + \frac{1}{\eta_c}\left(\pi_c^{(k-1)/k} - 1\right)\right] \tag{8}$$

where k is the specific heat ratio; π_c is the current section pressure ratio; T_{out} and T_{in} are the outlet and inlet temperatures of the pressurizer of the section, respectively; η_c is the modified adiabatic compression efficiency.

Expression for the power P_c consumed by each pressurized segment is:

$$P_c = G_{air}\left(h_{out} - h_{in}\right) \tag{9}$$

where G_{air} is the airflow through the current section of the pressurizer, h_{out} and h_{in} are the enthalpy of the outlet and inlet air of the current section of the pressurizer, respectively. The expression for the pumping volume is as follows:

$$\frac{G_{out}\sqrt{T_{in}}}{P_{in}} = K_{out}\sqrt{1-\frac{P_{out}}{P_{in}}} \tag{10}$$

According to the law of momentum, the following is obtained:

$$J\frac{d\omega}{dt} = M_t - M_c - M_m - M_{load} \tag{11}$$

where M_m and M_{load} are the mechanical loss torque and load torque, respectively.

As P=$M\omega$, the substitution into Eq. (9) leads to:

$$\frac{dn}{dt} = \frac{900}{J\pi^2 n}\left(P_t - P_c - P_m - P_{load}\right) \tag{12}$$

where: P_m, P_{load} for mechanical loss power and load loss power, J for the rotor moment of inertia.

As from Figure 2, the electric energy required by offshore oil production systems comes from the gas turbine and wind generator. The power grid is similar to the distribution system onshore. It contains two power sources and one power supply bus. There are three radial distribution feeders connected to the bus. The topology is shown in Figure 2 below. As shown in the below, the system contains three radial distribution feeders. The electrical load is connected to the remote end of the feeder. Each load represents the platform. The lenght of cable, which is a cross-linked polyethylene (XLPE) submarine cable, is shown in the Figure 2. The wind generator is interconnected to the bus of the platform.

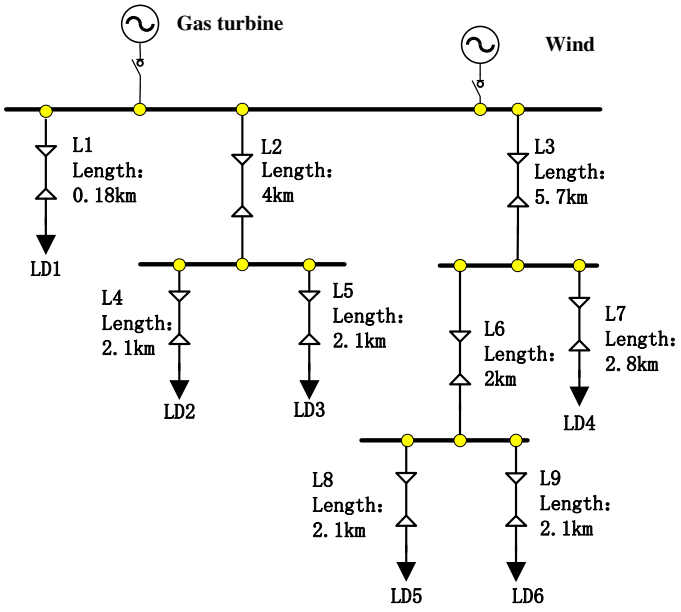

Fig. 2 *Offshore oil platform power grid topology*

As from Figure 3, the power grid load is connected to the remote terminal of the feeder. The transmission line uses an equivalent circuit. For the high impedance fault, the Cassie equivalent model is used. The capacity of the system is *33.48 MVA*. The submarine cable is modeled with the Bergeon model with distribution parameters.

The wind generator uses a fully rated converter based on permanent magnet synchronous wind turbines (PMSG), as used in the offshore oil microgrid [18-20]. Figure 3 shows the diagram of the wind generators. In Figure, wind turbines and power generators are used to produce power and the power electronic converter transmits the power to the power grid.

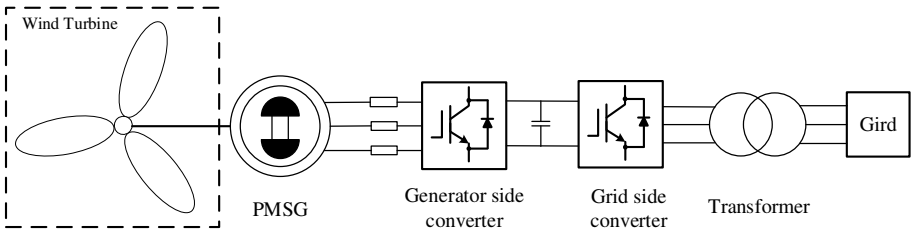

Fig. 3 *Wind generator diagram*

The control system of the wind turbine side is shown in Figure 4, and the converter on the machine side generates different control signals by controlling the PWM generator through the current inner loop and the voltage outer loop controller, so that the voltage and current output by the wind turbine can be controlled [21].

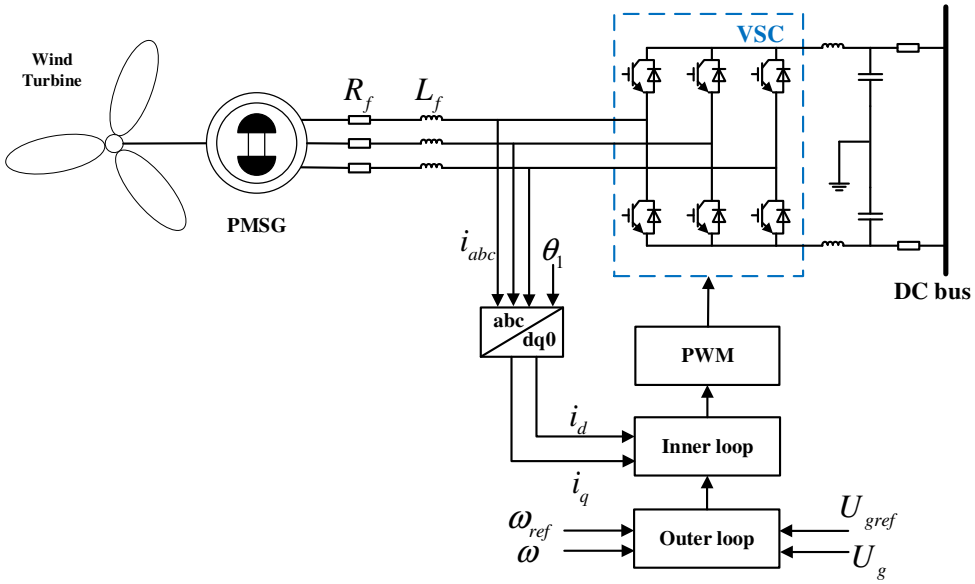

Fig. 4 *Diagram of the wind generator control system*

4. FAULT CHARACTERISTICS OF ARC FAULT

When a fault occurs at offshore oil and gas platsfom, the sequence network of the offshore power grid during fault can be illustrated as in the Figure 5 below where:

$Z_{Lk}^{(m\sim n)}$ is transmission line impedance from the *mth* platform to the *nth* platform,

$Z_{Ck}^{(m\sim n)}$ is transmission line capacitance from the *mth* platform to the *nth* platform,

$Z_{Dk}^{(m\sim n)}$ is load impedance from the *mth* platform to the *nth* platform,

$I_k^{(m)}$ is sequence current in the system from the *mth* node to the next node,

The term *k=0* represents the zero sequence, and *k=1* represents the positive sequence. *k=2* represents the negative sequence.

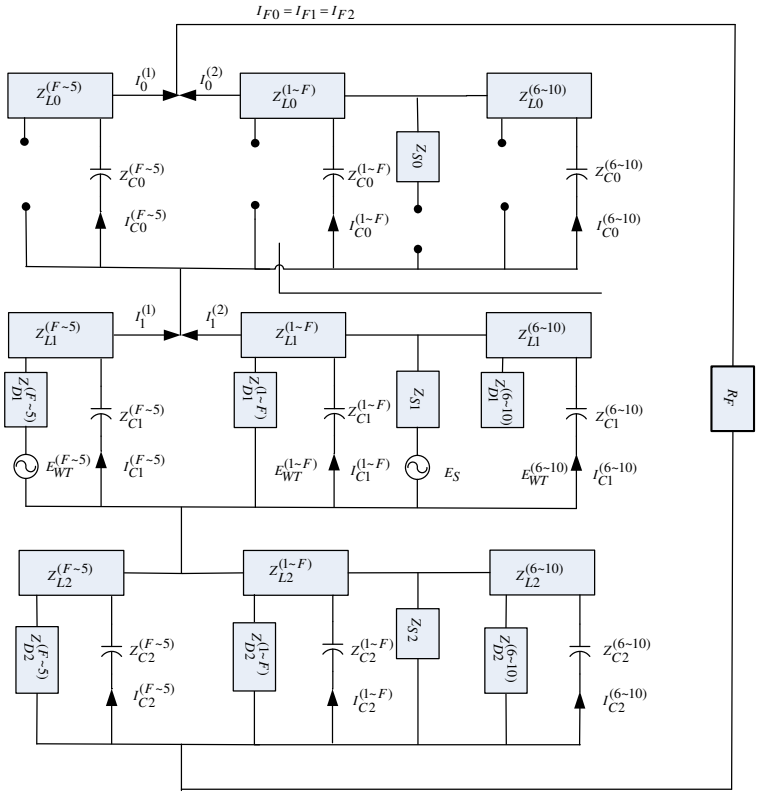

Fig. 5 *Interconnection of the sequence system for the SLG fault*

Figure 6 shows the simplified zero-sequence equivalent diagram of the power grid after the fault, using the sequence network processing and simplifying method. In the network, there is only the zero sequence part that showsthe relationship of each component. For the system with no grounding point at the neutral point, after a fault occurs, the positive- and negative-sequence part can be ignored since it does not affectthe correctness of the results. An arc fault occurs at platform 2, the measurement information is taken and processed at node 1 and node 3. Since the measurement direction of zero sequence current is reversed, the angle of I_0 leads to V_0 at node 1 and lags behind the V_0 at platform 3.

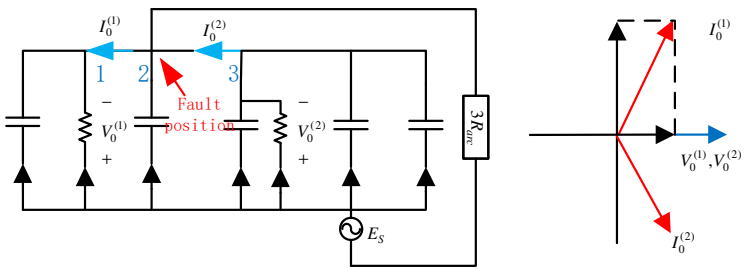

Fig. 6 *Simplified sequence networks for the arc fault*

When the arc fault happens inside the line, the electrical information measures are taken. On one side, the I_0 leads the voltage, and the polarity is 1, and on another, the I_0 lags the V_0, and the polarity is -1. If zero sequence angle polarity is different, it means there is arc fault inside the line. The flowchart of the proposed fault detection method is illustrated in Figure 7.

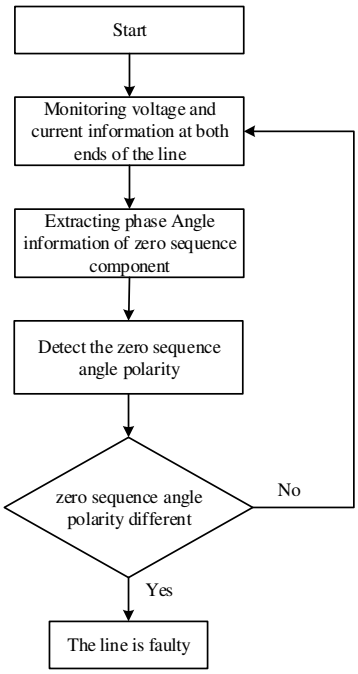

Fig. 7 *Arc fault detection flowchart*

5. CASE STUDY

The offshore oil platform power grid is simulated with PSCAD. As shown in Figure 8, the gas turbine is modeled using mathematical modelling, the wind generator using a power electronic interface and the arc fault using variable resistors. The voltage and current measurement positions are located at both sides of the arc fault line.

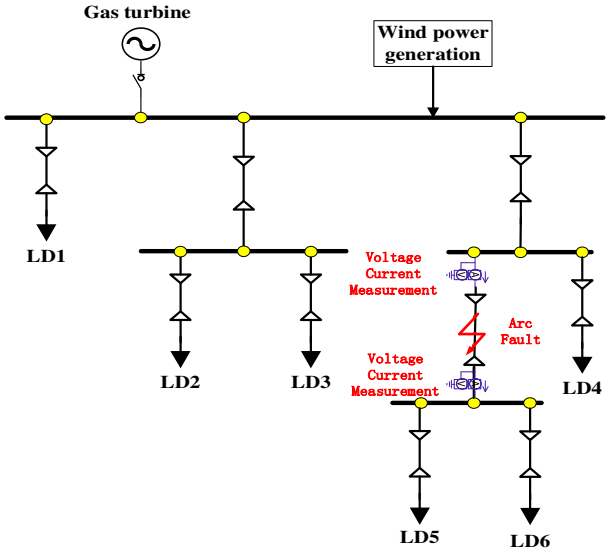

Fig. 8 *Schematic diagram of the simulation mode*

The simulation model uses the parameters as shown in Table 1.

Table 1 *Power grid parameter.*

Name	*Values*
Bus rated voltage	*10.5 kV*
Capacity (Gas turbine)	*40 MVA*
Capacity (Wind generator)	*5 MVA*
Capacity (Load)	*33.481 MW*

In the oil and gas platform, the PMSG generator produces power and sends it to the power grid. The output characteristics are shown in Figure 9. When the system is started, the gas turbine reacts quickly to provide electricity for the system, in about *0.1 s* of the peak power. Then with the increase in the power of the wind turbine, the power of the gas turbine decreases in about *0.4 s* of the gas turbine and the wind generator output balance. The power produced by the gas generator is *28.3 MW* and by the wind generator is *4.3 MW*.

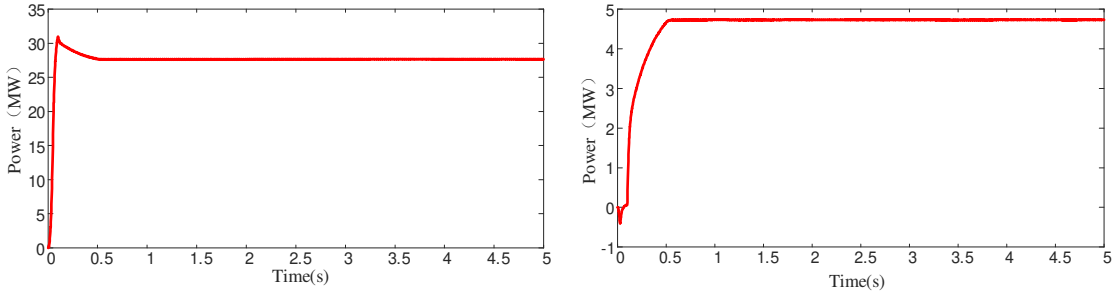

Fig. 9 *Generator output: (a) Gas turbine output power; (b) Wind generator output power*

With the access to wind generator, the power quality of the interconnection point should be studied. When the system is stable, the voltage and current waveform at the distributed energy access point are as shown in Figure 10 below.

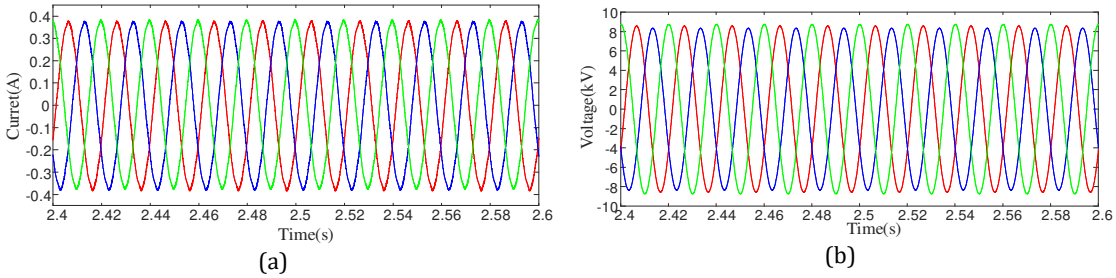

Fig. 10 *Characteristics of wind generator output: (a) Three-phase current; (b) Three-phase voltage*

Figure 11 illustrates the electrical component waveforms at the measurement point when the high impedance arc grounding fault occurs. Figure 11 (a) shows the changing characteristics of the fault voltage. When the arc is not generated, the air resistance between the fault point and the earth is large and the arc end voltage is high. When the arc is generated, the air between the fault point and the ground is broken, and the resistance is reduced. As the AC voltage crosses the peak and gradually decreases, the strength of the electric field decreases, and the active degree of the conductive medium decreases, resulting in an increased resistance and a small rise of the voltage. When the voltage enters the reverse change, the resistance is consistent with the forward direction. Figure 11 (b) shows the current changing characteristics. The current

changes inversely to the resistance increase. The voltage and the resistance decrease, and the current increases.

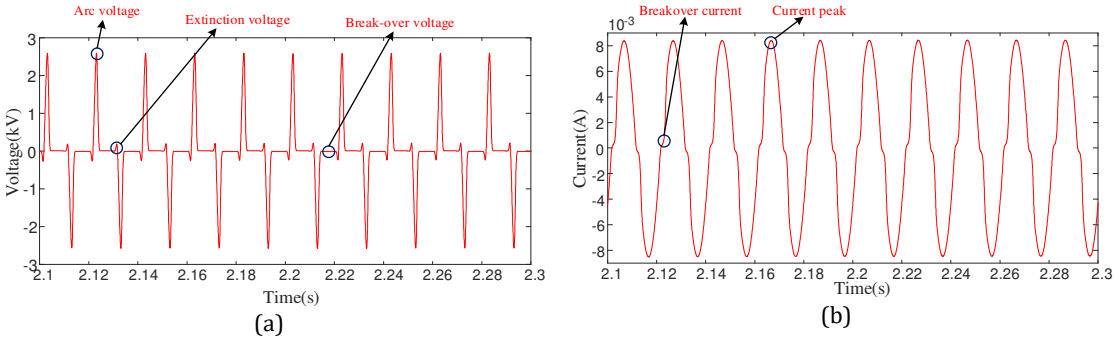

Fig. 11 *Arc voltage and current characteristics: (a) Voltage characteristic; (b) Current characteristics*

The arc grounding fault point in this simulation system is located on the feeder connected between the bus M3 and M4. As shown in Figure 12, multi-function meters are installed on both sides of the fault position. The measurement information after the fault is shown.

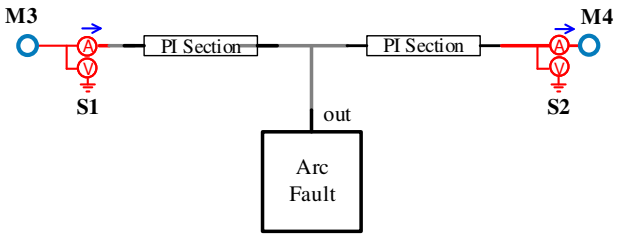

Fig. 12 *Arc ground fault position*

When an arc grounding fault happens in the line, the electrical information in the multifunctional meter S1 on the bus M3 is extracted and processed with the symmetric component method. Then the V_0 and I_0 information on the bus M3 are obtained, as shown in Figure 13. In the zero-sequence current, the arc extinguishes nearthe zero crossing point.

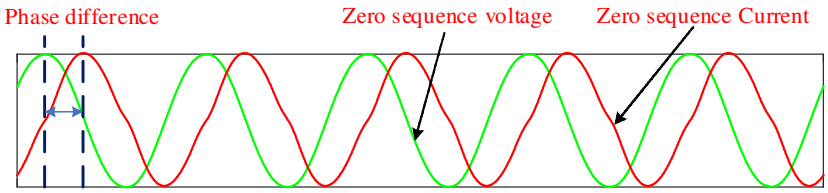

Fig. 13 *Zero sequence component at S1 during an internal fault*

When an arc grounding fault happens in the line, the voltage and current information in the multifunctional meter S2 on the bus M4 is extracted and processed with the symmetric component method. The V_0 and I_0 information on bus M4 after the fault are shown in Figure 14.

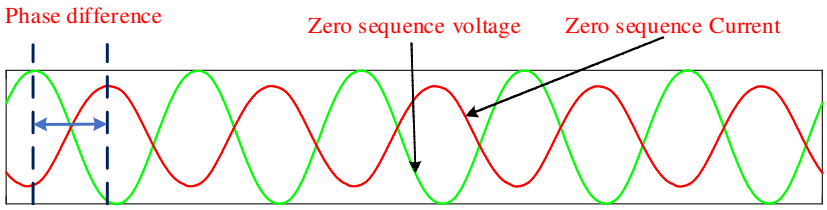

Fig. 14 *Zero sequence component at position S2 during an internal fault*

Figure 15 shows the flow direction of $I_{f(0)}$ emitted by the fault point when an arc grounding fault happens, pointing to bus M3 and bus M4 through the fault, respectively, with $I_{f(0)}=I_{f1(0)}+I_{f2(0)}$. The zero-sequence current $I_{f1(0)}$ flowing to the bus M3 is opposite to the measured direction of the multifunctional meter, so $I_{f1(0)}$ is negative; the zero-sequence current $I_{f2(0)}$ flowing to the bus M4 is opposite to the measured direction of the multifunctional meter, so the zero sequence current is positive.

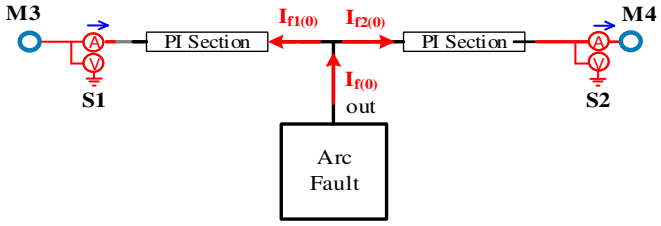

Fig. 15 *Schematic diagram of the internal faul*

Measuring the voltage and current data at S1 and S2, the zero-sequence voltage and current were obtained using the symmetric component method, as shown in Figure 12 and Figure 13, with the phase angle of each component extracted for making the difference. The angle difference between V_0 and I_0 at S1 and S2 is shown in Figure 16 (a) and Figure 16 (b).

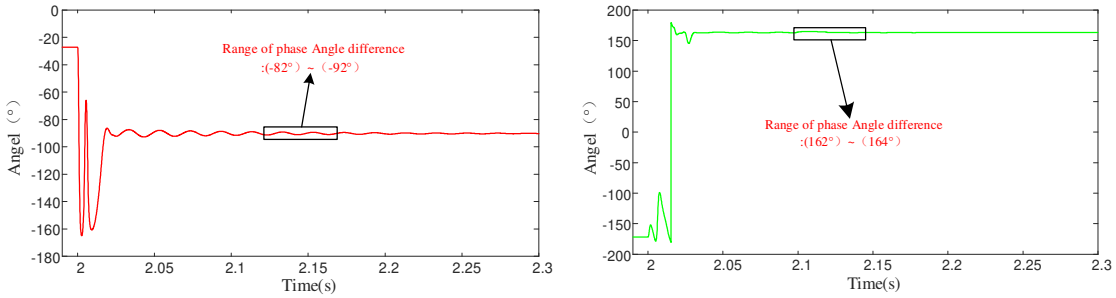

Fig. 16 *Internal fault angle difference: (a) Angle difference between V_0 and I_0 at position S1; (b) Phase angle difference between V_0 and I_0 at position S2*

When the fault occurs outside bus M3 and M4, the fault point occurs between bus M1 and bus M3, as shown in Figure 17. At this time, the flow direction of the zero sequence current $I_{f(0)}$ emitted by fault position is shown in the Figure below, flowing through the fault point to bus M1 and bus M3, respectively, with $I_{f(0)}=I_{f1(0)}+I_{f2(0)}$.The zero sequence current $I_{f2(0)}$ flows from bus M3 to bus M4 through nodes S1 and S2.

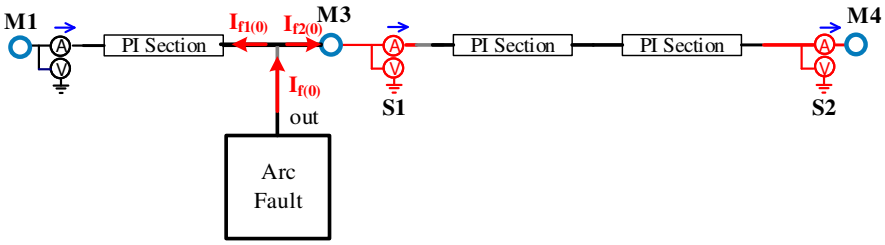

Fig. 17 *Schematic diagram of the external faults*

Similar to the internal fault handling method, the voltage and current information are presented in the multi-function tables S1 and S2, and the external fault is extracted and processed to obtain

the zero-order component. The electrical information on us M3 is obtained and shown in Figure 18. The zero sequence electrical information on bus M4 is obtained and illustrated in Figure 19.

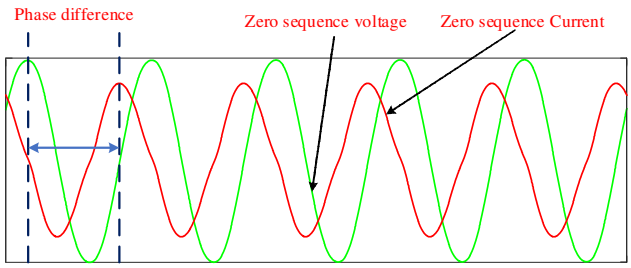

Fig. 18 *Zero-sequence component at position S1 during an external fault*

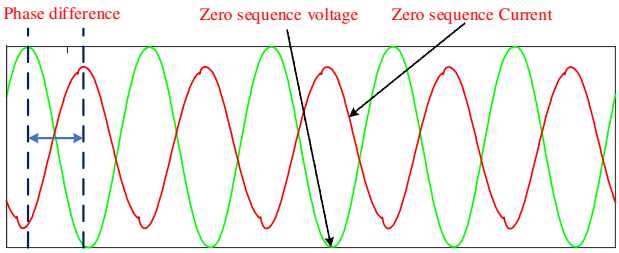

Fig. 19 *Zero-sequence component at position S2 during an external fault*

Similar to the method of handling the fault internally, the angle of the V_0 and I_0 at S1 and S2 is extracted, as shown in Figure 20, with different phase angles of the zero sequence component in the same position. The phase-angle difference between the V_0 and I_0 at node S1 is shown in Figure 20 (a). The phase-angle difference between the V_0 and I_0 at node S2 is shown in Figure 20 (b).

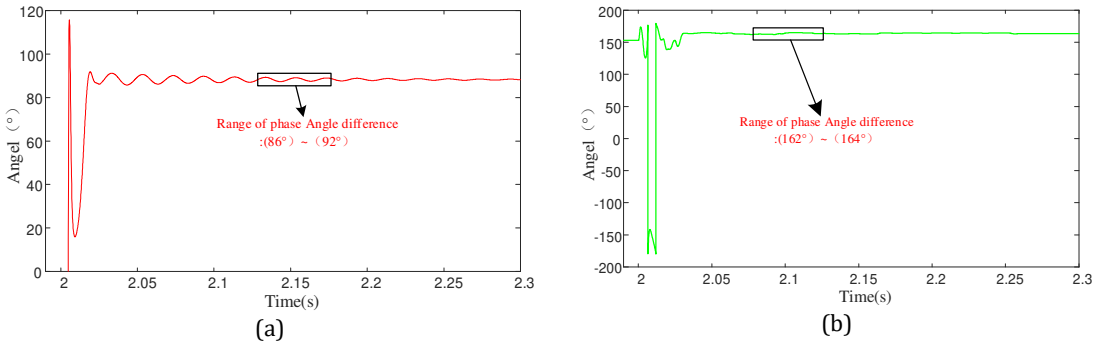

(a) (b)

Fig. 20 *External fault zero-sequence phase angle difference: (a) Phase angle difference at position S1; (b) Phase angle difference at position S2*

According to the two Figures above, the phase angle difference during fault occurs between the internal and external lines, which meets the proposed arc fault protection method.

6. CONCLUSION

In this paper, the mathematical model and electromagnetic transient simulation model of Cassie arc fault were studied and the characteristics of high-impedance arc fault are extracted. An improved arc fault detection method using the phase difference between the zero sequence

voltage and current was proposed. This method has little detection information and high accuracy, which solves the problem of small current and voltage changes in high resistance faults. The offshore oil platform power grid and arc fault were modeled using electromagnetic transient software PSCAD/EMTDC. The simulation results show that the arc model and fault detection method work well.

7. REFERENCES

[1] Q. Yu, Z. Jiang, Y. Liu, L. Li and G. Long, Optimization of an Offshore Oilfield Multi-Platform Interconnected Power System Structure, in IEEE Access, Vol. 9, pp. 5128-5139, 2021.

https://doi.org/10.1109/ACCESS.2020.3048980

[2] P.V. Dhawas, P.P. Bedekar and P.V. Nandankar, Advancement in Radial Power Distribution Network Using High impedance fault Relay, 2020 IEEE 17th India Council International Conference (INDICON), New Delhi, India, 2020, pp. 1-6.

https://doi.org/10.1109/INDICON49873.2020.9342171

[3] A. Nakho, K. Moloi and Y. Hamam, High Impedance Fault Detection Based on HS-Transform and Decision Tree Techniques, 2021 Southern African Universities Power Engineering Conference/Robotics and Mechatronics/Pattern Recognition Association of South Africa (SAUPEC/RobMech/PRASA), Potchefstroom, South Africa, 2021, pp. 1-5.

https://doi.org/10.1109/SAUPEC/RobMech/PRASA52254.2021.9377236

[4] S. Jin, W. Zhao, J. Ji and D. Xu, Deadbeat Fault-Tolerant Control Scheme for Dual Three-Phase PMSG With High-Resistance Connection Fault, in IEEE Transactions on Power Electronics, Vol. 38, No. 3, pp. 4015-4026, 2023.

https://doi.org/10.1109/TPEL.2022.3219544

[5] J. Hang, H. Wu, S. Ding, W. Hua and Q. Wang, A DC-flux-injection method for fault diagnosis of high-resistance connection in direct-torque controlled PMSM drive system, in IEEE Trans on Power Electron, Vol. 35, No. 3, pp. 3029–3042, 2020.

https://doi.org/10.1109/TPEL.2019.2924929

[6] J. Hang, J. Zhang, S. Ding, Y. Huang and Q. Wang, A model-based strategy with robust parameter mismatch for online HRC diagnosis and location in PMSM drive system, in IEEE Trans on Power Electron, Vol. 35, No. 10, pp. 10917–10929, 2020.

https://doi.org/10.1109/TPEL.2020.2978139

[7] S. Li and Y. Yan, Fault Arc Detection Based on Time and Frequency Domain Analysis and Radom Forest, 2021 International Conference on Computer Network, Electronic and Automation (ICCNEA), Xi'an, China, 2021, pp. 248-252.

https://doi.org/10.1109/ICCNEA53019.2021.00062

[8] C. Fontana, Fractal Dimension Logarithmic Differences Method for Low Voltage Series Arc Fault Detection, 2021 5th International Conference on Smart Grid and Smart Cities (ICSGSC), Tokyo, Japan, 2021, pp. 77-81.

https://doi.org/10.1109/ICSGSC52434.2021.9490436

[9] M. Jalil, H. Samet, T. Ghanbari and M. Tajdinian, An Enhanced Cassie–Mayr-Based Approach for DC Series Arc Modeling in PV Systems, in IEEE Transactions on Instrumentation and Measurement, Vol. 70, pp. 1-10, 2021, Art no. 9005710.

https://doi.org/10.1109/TIM.2021.3124832

[10] Z. Zhang, X. Fan, S. Liu, J. Xue, H. Yang and T. Luo, Research on DC Series Arc Model in Photovoltaic System Based on the Cassie Model, 2021 International Conference on Advanced Electrical Equipment and Reliable Operation (AEERO), Beijing, China, 2021, pp. 1-6. https://doi.org/10.1109/AEERO52475.2021.9708163

[11] M.N. Elfikky, A. El-Morshedy and M. El-Shahat, Arc Parameters and Fault Impedance effect on the Gradient of Arc Current and Rate of Rise of Recovery Voltage in HVDC Circuit Breaker Using Mayr Arc Model, 2021 IEEE AFRICON, Arusha, Tanzania, United Republic of, 2021, pp. 1-7. https://doi.org/10.1109/AFRICON51333.2021.9570846

[12] Q. Yu, Z. Jiang, Y. Liu, L. Li and G. Long, Optimization of an Offshore Oilfield Multi-Platform Interconnected Power System Structure, in IEEE Access, Vol. 9, pp. 5128-5139, 2021. https://doi.org/10.1109/ACCESS.2020.3048980

[13] K. Zhong, W. Chen and T. Zheng, Modeling and Fault Characteristic Analysis of an Offshore Multi-Platform Interconnected Power System, 2019 22nd International Conference on Electrical Machines and Systems (ICEMS), Harbin, China, 2019, pp. 1-5.

https://doi.org/10.1109/ICEMS.2019.8922382

[14] L.F.N. Lourenço, D.F. Pereira, R.M. Monaro, M.B.C. Salles and R.M.P. Rosa, Assessment of an Isolated Offshore Power Grid Based on the Power Hub Concept for Pre-Salt Oil and Gas Production, in IEEE Access, Vol. 10, pp. 87671-87680, 2022.

https://doi.org/10.1109/ACCESS.2022.3199761

[15] G. d. Alvarenga Ferreira and T. Mariano Lessa Assis, A Novel High Impedance Arcing Fault Detection Based on the Discrete Wavelet Transform for Smart Distribution Grids, 2019 IEEE PES Innovative Smart Grid Technologies Conference - Latin America (ISGT Latin America), Gramado, Brazil, 2019, pp. 1-6.

https://doi.org/10.1109/ISGT-LA.2019.8895264

[16] M. Wei, F. Shi, H. Zhang, F. Yang and W. Chen, A High-Efficiency Method to Determine Parameters of High Impedance Arc Fault Models, in IEEE Transactions on Power Delivery, Vol. 37, No. 2, pp. 1203-1214, 2022.

https://doi.org/10.1109/TPWRD.2021.3080280

[17] Y. Qingguang, Z. Weihuan, J. Zhicheng, L. Gaoxiang, L. Yuming and Z. Jiahe, NOVEL STRUCTURE OF POWER GRID OF OFFSHORE OIL PLATFORM GROUP, The 16th IET International Conference on AC and DC Power Transmission (ACDC 2020), Online Conference, 2020, pp. 2366-2369. https://doi.org/10.1049/icp.2020.0266

[18] Y. Sheng, C. Li, H. Jia, B. Liu, B. Li and T. A. Coombs, Investigation on FRT Capability of PMSG-Based Offshore Wind Farm Using the SFCL, in IEEE Transactions on Applied Superconductivity, Vol. 31, No. 8, pp. 1-4, 2021, Art no. 5604704.

https://doi.org/10.1109/TASC.2021.3091054

[19] Y. Fu, Z. Ren, S. Wei, Y. Xu and F. Li, Using Flux Linkage Difference Vector in Early Inter-Turn Short Circuit Detection for the Windings of Offshore Wind DFIGs, IEEE Transactions on Energy Conversion, Vol. 36, No. 4, pp. 3007-3015, 2021.

https://doi.org/10.1109/TEC.2021.3073007

[20] W. Gul, Q. Gao and W. Lenwari. Optimal Design of a 5-MW Double-Stator Single-Rotor PMSG for Offshore Direct Drive Wind Turbines, in IEEE Transactions on Industry Applications, Vol. 56, No. 1, pp. 216-225, 2020.

https://doi.org/10.1109/TIA.2019.2949545

[21] G. Ghanavati and S. Esmaeili, Dynamic simulation of a wind fuel cell hybrid power generation system, 2009 World Non-Grid-Connected Wind Power and Energy Conference, Nanjing, China, 2009, pp. 1-4.

https://doi.org/10.1109/WNWEC.2009.5335762